Adaptive Mixed-Form Fast Multipole Method for the Analysis of Electromagnetic Scattering

H. Chen, Z. H. Fan, R. S. Chen, Z. N. Jiang, and M. M. Li

Department of Communication Engineering
Nanjing University of Science and Technology, Nanjing, China, 210094
eechenrs@mail.njust.edu.cn

Abstract- To analyze an electrically large object with local fine structures, the conventional mixed form fast multipole algorithm requires that the boxes of the finest level are all with the same size, which belongs to the low-frequency region. This scheme is deficient since the mesh size is limited by the box size of the finest level, which is related to the finest parts of the object. In this paper, an efficient adaptive grouping scheme is introduced into a mixed-form fast multipole algorithm. In an adaptive mixed-form fast multipole algorithm, the number of unknowns in each non-empty box of the finest level is almost the same which results in the box of the finest level may be in a different frequency regime with a different size. Hence multipole expansions are employed, if the boxes located in the low frequency regime while the plane wave expansions are employed if the boxes located in the mid-frequency regime. Numerical results are given to show that the proposed approach is efficient to analyze the objects with many fine structures.

Index Terms- Adaptive grouping scheme, electromagnetic scattering, mixed-form fast multipole algorithm, multilevel fast multipole algorithm (MLFMA).

I. INTRODUCTION

The integral equation formulation is one of the most commonly used methods for solving the Maxwell's equations in electromagnetic scattering problems. Due to the fast increasing capability of computers, computational electromagnetics has developed to be more and more powerful. As a result, a number of algorithms have been presented for the fast computation of the large linear matrix equation systems resulting from the discretization of integral equations for electromagnetic scattering, such as conjugate gradient fast Fourier transform (CG-FFT) [1], adaptive integral method (AIM) [2], multilevel fast multipole algorithm (MLFMA) [3], etc.

Although many methods can simulate EM field accurately of electrically large objects, it remains to be difficult to simulate the EM field accurately where the size of the subscatterers is a small fraction of a wavelength. Many traditional methods suffer from a so-called "low frequency breakdown", such as method of moments (MoM), finite element method (FEM) and so on [3]. In order to capture the fine details of the structure accurately, e.g., in circuit components such as inductors and capacitors, this problem becomes more and more important and poses a pressing to simulate EM phenomena in circuits and antennas. Therefore, it becomes a popular topic for researchers in this field to overcome the low-frequency breakdown problem. Some fast methods have been proposed to cover the regime from low frequency to mid frequency, such as loop and tree basis decomposition introduced for EFIE [15, 16], the plane wave methods based on the generalized Gaussian quadrature rules proposed by Greengard [4], and the low-frequency fast inhomogeneous plane wave algorithm (LF-FIPWA) for wide-band fast computations [5, 6]. However, much memory is required for LF-FIPWA, since evanescent waves are highly direction dependent.

The fast multipole algorithm is numerically unstable due to the oscillatory characteristic of the spherical Hankel function for small arguments. As an attempt for a possible remedy, the mixed-form fast multipole algorithm (MF-FMA) [3, 7] is proposed to cover a wide band from the

low-frequency to mid-frequency. However, it is noticed that the MF-FMA need to construct multipole expansions for each nonempty boxes at the low frequency regime [3, 7]. As a result, the finest level boxes' size will all be less than 0.2λ ("λ" stands for wavelength). This results in a source distribution of high-density for the whole object. However, AMF-FMA just applies MF-FMA for some part of the object which belongs to the low frequency regime and the rest of the object which belongs to the mid frequency regime is still analyzed by MLFMA. Hence for an object containing fine structure, AMF-FMA takes advantage of adaptive grouping scheme [8, 13] to set the finest level box size smaller than 0.2λ for fine structure while for the rest of the object, the finest level box size is larger than 0.2λ. This frees MLFMA from low-frequency breakdown. As a result, the characteristics of both long-wavelength and short-wavelength are considered simultaneously for the object. In this way, the proposed algorithm is memory efficient since the adaptive grouping scheme is used.

This paper is organized as follows. Section II gives a brief introduction to the processing of near interaction of MF-FMA and the EFIE formulation in electromagnetic wave scattering. Section III describes the theory and implementation of the adaptive MF-FMA in more details. Numerical experiments with a few electromagnetic wave scattering problems are presented to demonstrate the efficiency of the AMF-FMA in Section IV. Section V gives some conclusions and comments.

II. EFIE FORMULATION

The EFIE formulation of electromagnetic wave scattering problems using planar Rao-Wilton-Glisson (RWG) basis functions for surface modeling is presented in [13]. The resulting linear systems from EFIE formulation after Galerkin's testing are briefly outlined as follows:

$$\sum_{n=1}^{N} Z_{mn} a_n = V_m, \qquad \mathrm{m} = 1, 2, ..., N, \qquad (1)$$

where

$$Z_{mn} = \frac{jk\eta}{4\pi} \iint_s \mathbf{f}_m(\mathbf{r}) \cdot \iint_s G(\mathbf{r}, \mathbf{r}') \mathbf{f}_n(\mathbf{r}') dS' dS$$

$$- \frac{j\eta}{4\pi k} \iint_s \nabla \bullet \mathbf{f}_m(\mathbf{r}) \cdot \iint_s G(\mathbf{r}, \mathbf{r}') \nabla \bullet \mathbf{f}_n(\mathbf{r}') dS' dS,$$

and

$$V_m = \int_s \mathbf{f}_m(\mathbf{r}) \cdot \mathbf{E}^i(\mathbf{r}) ds, \quad G(\mathbf{r}, \mathbf{r}') = \frac{e^{-jk|\mathbf{r}-\mathbf{r}'|}}{4\pi |\mathbf{r}-\mathbf{r}'|}.$$

Here, $G(\mathbf{r}, \mathbf{r}')$ refers to the Green's function in free space and $\{a_n\}$ is the column vector containing the unknown coefficients of the surface current expansion with RWG basis functions. Also, as usual, $\mathbf{r}$ and $\mathbf{r}'$ denote the observation and source point locations. $\mathbf{E}^i(\mathbf{r})$ is the incident excitation plane wave, and η and k denote the free space impendence and wave number, respectively. Once the matrix equation (1) is solved by numerical matrix equation solvers, the expansion coefficients $\{a_n\}$ can be used to calculate the scattered field and RCS. In the following, we use $\mathbf{A}$ to denote the coefficient matrix in equation (1), $\mathbf{x} = \{a_n\}$, and $\mathbf{b} = \{V_m\}$ for simplicity. Then, the EFIE matrix equation (1) can be symbolically rewritten as:

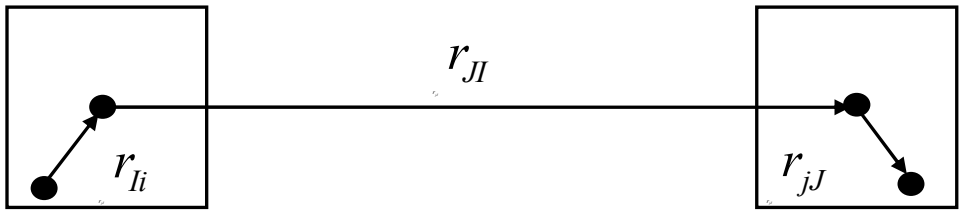

Fig. 1. The general translation used for LF-FMA.

$$\mathbf{Ax} = \mathbf{b}. \qquad (2)$$

To solve the above matrix equation by an iterative method, the matrix-vector products are

needed at each iteration. Physically, a matrix-vector product corresponds to one cycle of interactions between the basis functions. The basic idea of the mixed-form FMA (MF-FMA) is to combine the LF-FMA with the MLFMA into one uniform expression and convert the interaction of element-to-element to the interaction of group-to-group. Here, a group includes the elements residing in a spatial box. The mathematical foundation of the mixed-form FMA is, also, the addition theorem for the scalar Green's function in free space. Using the MF-FMA, the matrix-vector product $\mathbf{Ax}$ can be written as:

$$\mathbf{Ax} = \mathbf{A}_N\mathbf{x} + \mathbf{A}_F\mathbf{x}.$$

Here, $\mathbf{A}_N$ is the near part of $\mathbf{A}$ and $\mathbf{A}_F$ is the far part of $\mathbf{A}$.

In the MF-FMA, the calculation of matrix elements in $\mathbf{A}_N$ remains the same as in the MoM procedure. However, those elements in $\mathbf{A}_F$ are not explicitly computed and stored. Hence, they are not numerically available in the MF-FMA.

III. ADAPTIVE MIXED-FORM FAST MULTIPOLE ALGORITHM

It is well known that the diagonalized translation matrix of the 3-D MLFMA can greatly decrease the memory requirements and expedite the matrix-vector multiplication. However, it can not avoid low-frequency breakdown [3, 4]. In order to overcome the low-frequency breakdown, the low-frequency fast multipole algorithm (LF-FMA) is developed [12] and it bridges the gap from static to electrodynamic.

A. Low-frequency fast multipole algorithm

As shown in Fig. 1, $\boldsymbol{r}_{ji} = \boldsymbol{r}_{jJ} + \boldsymbol{r}_{JI} + \boldsymbol{r}_{Ii}$ and the addition theorem [3, 9, 10] is utilized for LF-FMA. The general translation equation is obtained as follows:

$$\alpha_{LL'}\left(\mathbf{r}_{ji}\right) = \sum_{L_1}\sum_{L_2}\beta_{LL_1}\left(\mathbf{r}_{jJ}\right)\alpha_{L_1L_2}\left(\mathbf{r}_{JI}\right)\beta_{L_2L'}\left(\mathbf{r}_{Ii}\right) \tag{3}$$

The above equation is a recursive equation and $L = (l, m), 0 \le l \le \mathrm{P}, -l \le m \le l$, P is truncation number of multipoles. Here, L_1, L_2 and L' have similar definitions as L. L and L' are used as the subscripts for the α operator and the β operator. $\alpha_{LL'}$ and $\beta_{LL'}$ are defined as

$$\alpha_{L',L}\left(\mathbf{r}\right) = \sum_{L''} 4\pi\left(-j\right)^{\left(l'+l''-l\right)}\Psi_{L''}\left(k,\mathbf{r}\right)A_{L,L',L''} \tag{4}$$

$$\beta_{L',L}\left(\mathbf{r}\right) = \sum_{L''} 4\pi\left(-j\right)^{\left(l'+l''-l\right)}\Re_g\Psi_{L''}\left(k,\mathbf{r}\right)A_{L,L',L''}, \tag{5}$$

where

$$\begin{aligned}\Psi_L\left(k,\mathbf{r}\right) &= h_l^{(2)}\left(kr\right)Y_l^m\left(\theta,\phi\right)\\ \Re_g\Psi_L\left(k,\mathbf{r}\right) &= j_l\left(kr\right)Y_l^m\left(\theta,\phi\right).\end{aligned} \tag{6}$$

$A_{L,L',L''}$ is the Gaunt coefficient, $h_l^{(2)}\left(x\right)$ is the spherical Hankel function of the second kind, $Y_l^m\left(\theta,\phi\right)$ is the spherical harmonic function [10, 11].

$G(\boldsymbol{r}_j, \boldsymbol{r}_i)$ is free space green's function and corresponds to $\alpha_{00}(\boldsymbol{r}_{ji})$

$$G\left(\mathbf{r}_j,\mathbf{r}_i\right) = -jk\alpha_{00}\left(\mathbf{r}_{ji}\right). \tag{7}$$

B. Adaptive mixed-form fast multipole algorithm

LF-MLFMA is developed for very low-frequency problems based on the non-diagonalized form of the fast multipole translator and the multipoles are efficient in grouping and translating waves among much smaller objects or boxes [3, 7]. However, LF-MLFMA will lose its accuracy and efficiency when the box size is above 0.2λ. Multipoles and plane waves are combined into one octree browsing process to form the MF-FMA for the efficient analysis in both low frequency and mid-frequency bands. When the frequency is low, or the MLFMA box sizes are small compared to wavelength, the non-diagonalized form of the fast multipole translator is used. When the box sizes are comparable to wavelength, the diagonalized form of the fast multipole (plane wave) translator is used for translation. In this manner, the

multilevel algorithm can efficiently work for box sizes to be a small fraction of a wavelength and the whole simulation objects can be electrically large enough when compared to wavelength.

The fast multipole translator $\alpha_{LL'}$ is always in the form of dense matrix and can be diagonalized into the plane wave integrations (8) and (9).

Inserting (9) into (3), the Mixed-form translation containing two-level multipoles translation and two-level diagonal translation in the form of matrix is obtained in (10) below, where S_i is a sample number of propagating waves over a unit sphere at a level for diagonal translations, [***I***] is the interpolation matrix and $[\boldsymbol{I}]^{\mathrm{T}}$ denotes the transpose of matrix [***I***]. J_i and I_i denote the different boxes in "i" level. "Diag" is short for the diagonal translation matrix. $[\boldsymbol{D}]_{S\times L}$ is transformer from multipoles to plane waves, and $\left[\boldsymbol{D}\right]^{\dagger}_{S\times L}$ is transformer from plane waves to multipoles [7].

$$\alpha_{LL'}\left(\mathbf{r}_{ji}\right)=\int d\Omega_k\left(-j\right)^{l}Y_L^{*}\left(\Omega_k\right)e^{-j\mathbf{k}\cdot\mathbf{r}_{JJ}}\tilde{T}_{JI}\left(\Omega_k,\boldsymbol{r}_{JI}\right)\left(-j\right)^{-l'}Y_{L'}\left(\Omega_k\right)e^{-j\mathbf{k}\cdot\mathbf{r}_{Ii}} \tag{8}$$

$$\tilde{T}_{JI}\left(\Omega_k,\Omega'_k\right)=\sum_{l=0}^{L_{\max}}\left(-j\right)^{l}\left(2l+1\right)h_{l''}^{(2)}\left(kr_{JI}\right)P_l\left(\hat{k}\bullet\hat{\boldsymbol{r}}_{\boldsymbol{JI}}\right) \tag{9}$$

$$\begin{aligned}\left[\alpha_{LL'}\left(\mathbf{r}_{ji}\right)\right]_{L\times L'}=&\left[\beta_{LL_1}\left(\mathbf{r}_{jJ_1}\right)\right]_{L\times L_1}\cdot\left[\beta_{L_1L_2}\left(\mathbf{r}_{J_1J_2}\right)\right]_{L_1\times L_2}\\&\cdot\left[\boldsymbol{D}\right]^{\dagger}_{S_3\times L_2}\cdot diag\left[e^{-j\mathbf{k}\cdot\mathbf{r}_{J_2J_3}}\right]_{S_3\times S_3}\cdot\left[\boldsymbol{I}\right]^{\mathrm{T}}_{S_4\times S_3}\cdot diag\left[e^{-j\mathbf{k}\cdot\mathbf{r}_{J_3J_4}}\right]_{S_4\times S_4}\\&\cdot diag\left[\tilde{T}\left(\Omega_{s4},\boldsymbol{r}_{J_4I_4}\right)\omega_{S_4}\right]_{S_4\times S_4}\\&\cdot diag\left[e^{-j\mathbf{k}\cdot\mathbf{r}_{I_4I_3}}\right]_{S_4\times S_4}\cdot\left[\boldsymbol{I}\right]_{S_4\times S_3}\cdot diag\left[e^{-j\mathbf{k}\cdot\mathbf{r}_{I_3I_2}}\right]_{S_3\times S_3}\cdot\left[\boldsymbol{D}\right]_{S_3\times L_2}\\&\cdot\left[\beta_{L_2L_1}\left(\mathbf{r}_{I_2I_1}\right)\right]_{L_2\times L_1}\cdot\left[\beta_{L_1L'}\left(\mathbf{r}_{I_1i}\right)\right]_{L_1\times L'}\end{aligned} \tag{10}$$

$$\begin{aligned}\frac{e^{-jkr_{ji}}}{r_{ji}}&=-jk\alpha_{00}\left(\mathbf{r}_{ji}\right)\\&=-jk\left[\beta_{0L_1}\left(\mathbf{r}_{jJ_1}\right)\right]_{1\times L_1}\cdot\left[\beta_{L_1L_2}\left(\mathbf{r}_{J_1J_2}\right)\right]_{L_1\times L_2}\\&\cdot\left[\boldsymbol{D}\right]^{\dagger}_{S_3\times L_2}\cdot diag\left[e^{-j\mathbf{k}\cdot\mathbf{r}_{J_2J_3}}\right]_{S_3\times S_3}\cdot\left[\boldsymbol{I}\right]^{\mathrm{T}}_{S_4\times S_3}\cdot diag\left[e^{-j\mathbf{k}\cdot\mathbf{r}_{J_3J_4}}\right]_{S_4\times S_4}\\&\cdot diag\left[\tilde{T}\left(\Omega_{S_4},\boldsymbol{r}_{J_4I_4}\right)\omega_{S_4}\right]_{S_4\times S_4}\\&\cdot diag\left[e^{-j\mathbf{k}\cdot\mathbf{r}_{I_4I_3}}\right]_{S_4\times S_4}\cdot\left[\boldsymbol{I}\right]_{S_4\times S_3}\cdot diag\left[e^{-j\mathbf{k}\cdot\mathbf{r}_{I_3I_2}}\right]_{S_3\times S_3}\cdot\left[\boldsymbol{D}\right]_{S_3\times L_2}\\&\cdot\left[\beta_{L_2L_1}\left(\mathbf{r}_{I_2I_1}\right)\right]_{L_2\times L_1}\cdot\left[\beta_{L_10}\left(\mathbf{r}_{I_1i}\right)\right]_{L_1\times 1}\end{aligned} \tag{11}$$

$$\frac{e^{-jkr_{ji}}}{r_{ji}} = diag\left[e^{-j\mathbf{k}\cdot\mathbf{r}_{J_jJ_3}}\right]_{S_3\times S_3}\cdot\left[\boldsymbol{I}\right]^{\mathrm{T}}_{S_4\times S_3}\cdot\ diag\left[e^{-j\mathbf{k}\cdot\mathbf{r}_{J_3J_4}}\right]_{S_4\times S_4}$$
$$\cdot\ diag\left[\tilde{T}\left(\Omega_{S_4},\mathbf{r}_{J_4I_4}\right)\omega_{S_4}\right]_{S_4\times S_4} \tag{12}$$
$$\cdot\ diag\left[e^{-j\mathbf{k}\cdot\mathbf{r}_{I_4J_3}}\right]_{S_4\times S_4}\cdot\left[\boldsymbol{I}\right]_{S_4\times S_3}\cdot\ diag\left[e^{-j\mathbf{k}\cdot\mathbf{r}_{I_3j}}\right]_{S_3\times S_3}.$$

The free space Green's function is expanded by mixed-form translation through equation (10) as (11) above, and the free space Green's function is expanded by plane wave translation for MLFMA as (10) above.

It can be found from the above equations that both the LF-MLFMA and the MF-FMA uses the same grouping structure as MLFMA. Therefore, the simulated object is first enclosed by the smallest possible box, called root boxes. Then the root box is divided into eight equal boxes and each of the child boxes is recursively subdivided into eight smaller boxes until we reach the finest level. For MF-FMA, when the multipole expansion is applied for each nonempty box in the finest level, it is inevitable to produce a large number of unknowns because of the source distribution for the whole object is high-density at the low-frequency regime and the number of the finest level box is consequentially larger than

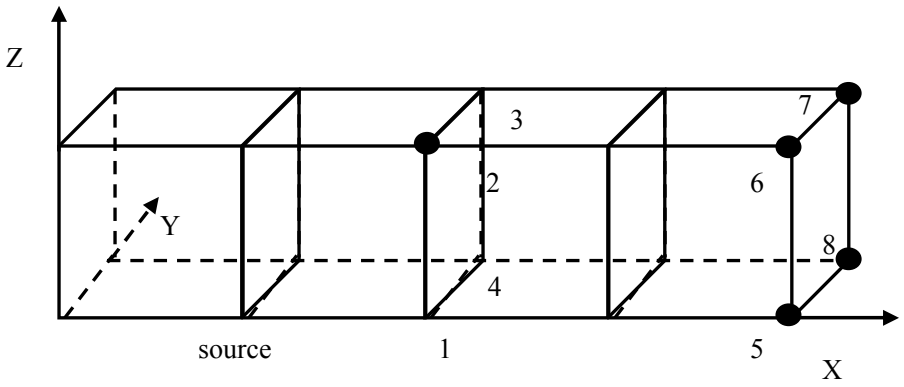

Fig. 2. Point positions.

MLFMA. Therefore, the MF-FMA is not necessary for the whole object but only used for the fine structures connected with the electrically large object.

In the conventional grouping scheme described above, the parent boxes are divided regardless of the number of sources inside them [9]. However, for some fraction of the object, the source distribution is high-density and it is in fact a low-frequency problem. As a result, the uniform partitioning often leads to the whole object divided with the same resolution and the simulation result is not accurate. When MF-FMA is used for the object, the box size of finest level can be smaller than 0.2λ, but source distribution is high-density for the whole object. To improve the efficiency of the method, the MF-FMA is applied for fine structures of the object which is considered at the low-frequency regime and the conventional MLFMA is used for the rest of the object which is considered in the mid-frequency regime. As MF-FMA and MLFMA is used at the same time, the size of leafy groups is not always the same. Therefore, a new grouping scheme has to be developed.

Different from the method described in [12], if a box doesn't contain sources in the low-frequency regime, it will be considered as a leaf box and the subdivision is terminated for that box, otherwise it will continue to be divided until satisfying the low-frequency grouping requirement. The following text gives a tree

structure where the leaf boxes can be in any of the refinement levels. The pseudocode of the adaptive tree construction is given as follows:

Algorithm I: Adaptive tree structure

Step 1: Enclose the sources in the smallest possible box (computational domain)

Step 2: Decompose the computational domain to eight equal child boxes

Step 3: For each child box k, **do** k = 1 to 8

Step 4: **If** it contains no source, **then** eliminate it,

Step 5: **If** it contains sources that belong to the mid-frequency regime and the box size is 0.2λ, **then**

Step 6: The box is considered a mid-frequency leaf box and is not further divided

Step 7: **end if**

Step 8: **else**

Step 9: Divide it into its 8 child boxes

Step 10: **end if**

Step 11: **end do**

Step 12: Repeat until the boxes at the finest level agree with the low-frequency requirement.

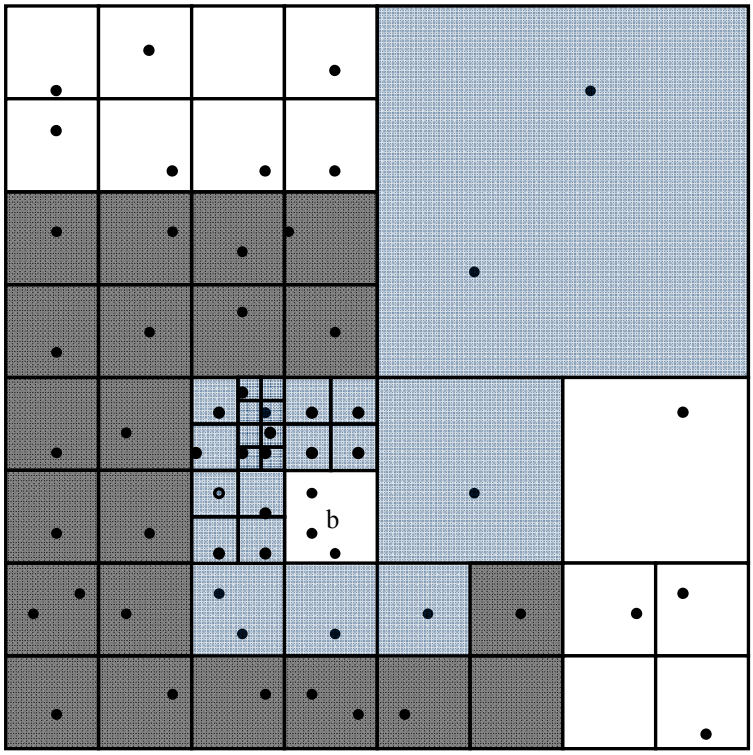

Fig. 3. Adaptive grouping.

In the adaptive scheme, the interaction sublists for the boxes are formed similar to the traditional fast multipole algorithm. As the leaf boxes can be in any of the refinement levels, the construction of the near list is more involved. To define the near list, we consider a box i at level l. The descents of box i are boxes in levels l_d, $l_d < l$, that are contained in box i. These include the children, grandchildren etc. of box i. The ancestors of box i are boxes in levels l_a, $l_a > l$, that contain box i.

For each leaf box b, we define the following sets of boxes:

1. The leaf boxes which are descents of box b's near neighbors, which is denoted by the set N_d.
2. The leaf boxes which are near neighbors of box b's ancestors, which is denoted by the set N_a.
3. The leaf boxes which are near neighbors of box b, denoted by the set N_n . The near list of a leaf box b consists of boxes b_n, where b_n belongs to $\{ N_n \cup N_a \cup N_d \}$.

As is shown in Fig. 3, the adaptive partitioning of the computational domain for a nonuniform distribution of sources is shown in two

dimensions. Consider a leaf box b, the boxes in the near list are lightly shaded, and the boxes in deep color are b's far groups.

Usually, the mesh density for the small cylinder is higher than the cubic for the object shown in Fig. 5. As a result, if the box size is set 0.2λ for the finest level, it will contain many elements in a box which results in large memory consumption for the near interaction matrix. To alleviate the press of near interaction, according to the adaptive grouping scheme in [8, 12] and making some modification as the above description, MF-FMA is applied for in the purple small cylinder and MLFMA is applied for in the cubic at the bottom. Thus, the finest level box size for the MF-FMA can be set smaller than 0.2λ while the finest level box size is at least 0.2λ for MLFMA.

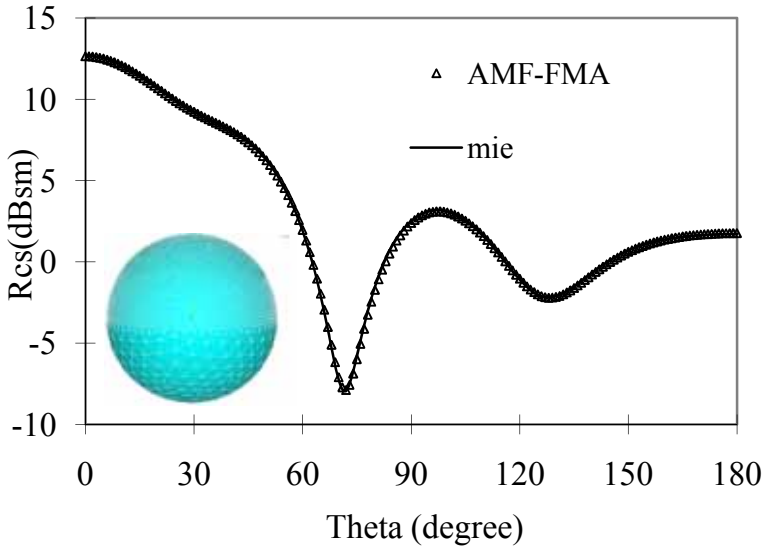

Fig. 4. Bistatic RCS of a PEC sphere working at 0.18 GHz simulated by Mie series and adaptive mixed-form FMA.

IV. NUMERICAL RESULTS

In this section, several numerical examples are presented to demonstrate the efficiency of adaptive MF-FMA (AMF-FMA) for fast analysis of electromagnetic scattering. All experiments are performed on a Core-2 6300 with 1.86 GHz CPU and 1.96GB RAM in single precision. The iteration process is terminated when the normalized backward error is reduced by 10^{-3} for all examples.

In the implementation of the MF-FMA, the adaptive grouping method is used to reduce the memory consumption and captures the fine details of the structure. The incident wave is considered to be a plane wave at $\theta = 0.0$, $\varphi = 0.0$. All geometries are modeled by plane triangles panels. As shown in Fig. 4, the numerical results of bistatic RCS for vertical polarization are given to illustrate the performance of our AMF-FMA. It consists of a sphere with radius 1m at 180MHz, and the average element size is 0.048 for the top half sphere with 3042 unknowns while the average element size is 0.06 for the bottom half sphere with 843 unknowns. The MF-FMA and MLFMA are applied to the top half sphere and the bottom, respectively. The numerical result of AMF-FMA is compared with the Mie series and we can see the result agrees with the Mie series vigorously.

In Fig. 6, the geometry is a cube connected with a small cylinder with 11862 unknowns. The size of the cube is 1m × 1m× 1m with a small cylinder whose radius is 0.03m and the height is 1m. The average element size is 0.03 for the small cylinder with 826 unknowns and the cubic is 0.043 at 300MHz. The numerical results of the

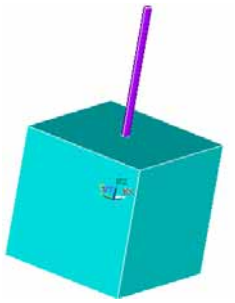

Fig. 5. A cubic with a small cylinder.

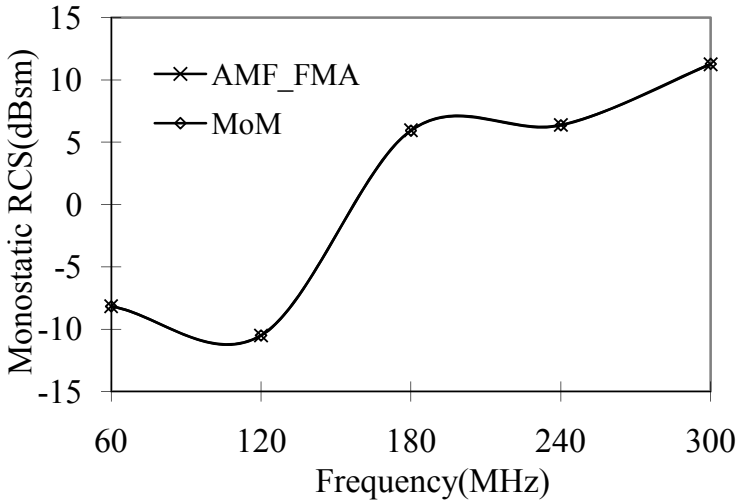

Fig. 6. Monostatic RCS of the cube-cylinder simulated by MoM and adaptive mixed-form FMA.

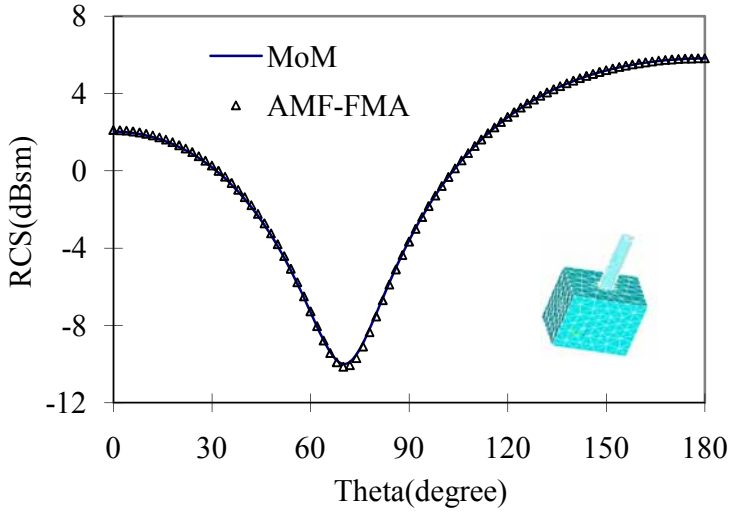

Fig.7. Bistatic RCS of the cube-cylinder working at 60MHz simulated by MoM and adaptive mixed-form FMA.

monostatic RCS for vertical polarization are given to illustrate the performance of our AMF-FMA at 60 MHz, 120 MHz, 180 MHz, 240 MHz, and 300MHz. The finest level box size corresponding to the frequencies is 0.05λ, 0.05λ, 0.15λ, 0.1λ, and 0.125λ.

Two levels LF-FMA is applied for the whole object at 60 MHz. Mixed-form translation containing two levels multipoles translation and one level diagonal translation is utilized for the small cylinder and the cubic is analyzed by one level MLFMA at 120 MHz. For 180 MHz and 240 MHz, mixed-form translation containing one level multipoles translation and one level diagonal translation is used for the small cylinder and the cubic is analyzed by one level MLFMA. At 300MHz, mixed-form translation containing one level multipoles translation and two levels diagonal translation is used for the small cylinder while the cubic is analyzed by two levels MLFMA.

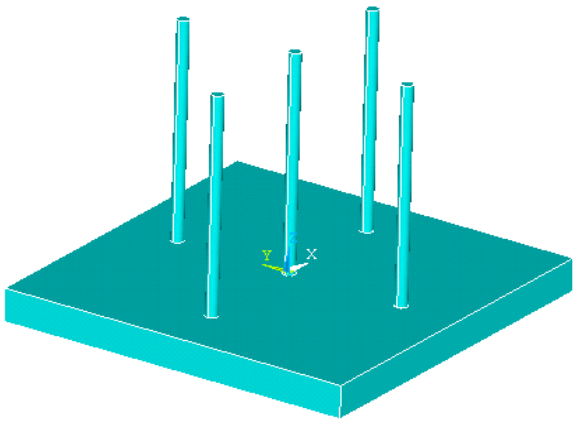

Fig. 8. A cuboid with many fine structures.

At 60 MHz, the electrical size of the cube-cylinder is 0.4λ and the average element size is 0.006 for the small cylinder and 0.0086 for the cubic. AMF-FMA degenerates to two levels LF-FMA with the finest level box size is 0.05λ. It is shown in Fig. 7 that the result has a good agreement with MoM.

When the proportion of fine structures in an object goes up as shown in Fig. 8, the total memory consumption for MLFMA and AMF-FMA is described in Fig. 9. The cuboid of the object in Fig. 8 is of the size 3m×3m×0.5m and the small cylinders are all in the same size with radius 0.05m and the height 2m. The average element size for the cuboid is around 0.093 and set the average element size for all cylinders varies from 0.033 to 0.01, corresponding with the unknowns from 8490 to 49011.The box size at the finest level for MLFMA is set 0.25λ. The finest level box sizes of AMF-FMA are 0.05λ for fine structures and 0.2λ for the rest of the object at 200 MHz. Using AMF-FMA for the object, MF-FMA is applied for the cylinders and MLFMA is for the cuboid. With the total number of unknowns increasing, it can be seen from Fig. 9(a) that the memory consumption of storage near part matrix

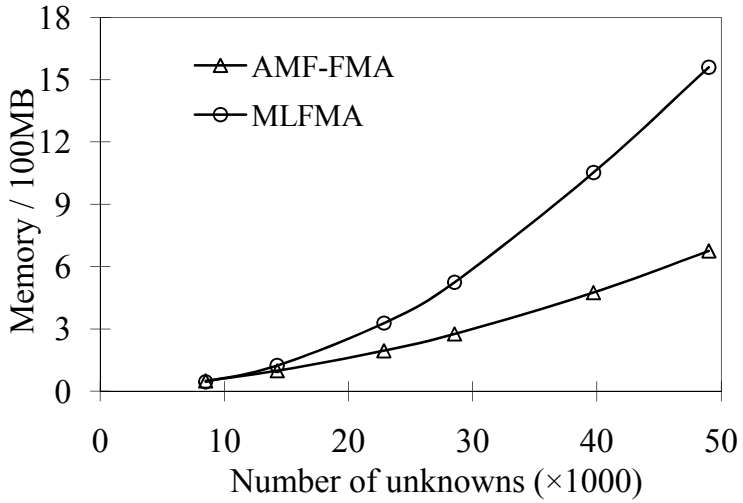

(a)

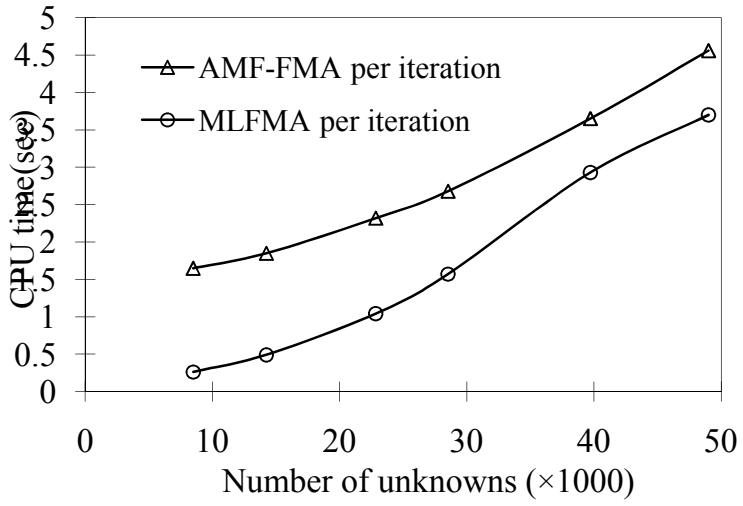

(b)

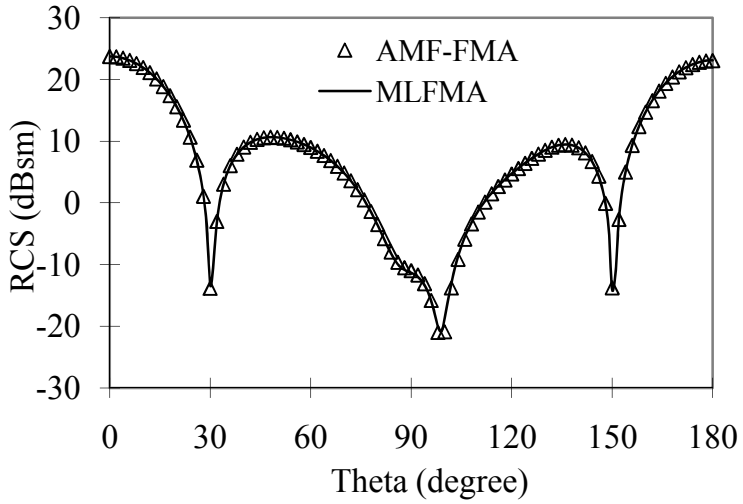

(c)

Fig. 9. (a) The memory consumption of the object shown in Fig. 8 between AMF-FMA and MLFMA, (b) CPU times for one matrix-vector operation versus the number of unknowns for the object shown in Fig. 8, and (c) bistatic RCS of the object shown in Fig. 8 simulated by MLFMA and AMF-FMA at 200MHz.

elements of $\mathbf{A}_N$ is large for MLFMA when leaf box size is 0.25λ. In other words, the more unknowns for the fine structures, the less memory requirement for AMF-FMA compared with MLFMA. In Fig. 9(b), it can be seen that the CPU time of AMF-FMA for one matrix-vector operation is more than MLFMA, but the CPU time consumption of AMF-FMA is close to MLFMA with the increasing of the unknowns for the fine structures. In Fig. 9(c), the bistatic RCS of the object in Fig. 8 for vertical polarization is given at 200 MHz with the unknowns 8490.

It can be seen from the figure that the result of AMF-FMA agrees with MLFMA vigorously.

Table 1: Test the LF-FMA translator

Source point	Field point	Green's function	Multipoles expansion
(0, 0, 0.)	(1.0, 0, 0.)	(0.9980267,-6.2790520E-02)	(0.9917871,-6.2790506E-02)
(0, 0, 0.)	(1.0,0.5,0.)	(0.8922212,-6.2780187E-02)	(0.8950982,-6.2780164E-02)
(0, 0, 0.)	(1.0,0.5,0.5)	(0.8140802,-6.2769860E-02)	(0.8088611,-6.2769853E-02)
(0, 0, 0.)	(1.0,0.,0.5)	(0.8922212,-6.2780187E-02)	(0.8950983,-6.2780179E-02)

Table 2: Test the MF-FMA translator

Source point	Field point	Green's function	Multipole expansion
(0.25,0,0)	(1,0.1,0)	(-0.4293182,-1.249964)	(-0.4293646,-1.249869)
(0.25,0,0)	(1,0.24,0.24)	(-0.5804493,-1.067079)	(-0.5811364,-1.066991)
(0.25,0,0)	(1.24,0.24,0.24)	(-0.8333122,-0.4675281)	(-0.8338917,-0.4674568)
(0.25,0,0)	(1.24,0,0.25)	(-0.8216858,-0.5328912)	(-0.8221112,-0.5328190)

In Tables 1 and 2, we test the accuracy of equation (6) and equation (10). In Table 1, we choose the leafy box size is 0.5m and the source point is located at (0, 0, 0.). We take field point at 1, 2, 3, 4, as shown in Fig. 2, the frequency is 0.003GHz. In Table 2, we choose the leafy box is 0.25m and the frequency is 0.12GHz. The source point is fixed at (0.25, 0, 0.) and the field points are selected at random. From the two tables, we can conclude that the error of the results is no more than 1%.

V. CONCLUSIONS

In this paper, we have described an adaptive grouping scheme combined with MF-FMA (AMF-FMA) for solving electromagnetic wave scattering problems. One advantage of our presented AMF-FMA is that it can cover a wide band from low frequency to mid-frequency without low-frequency breakdown. Another improvement is that for the object with fine structures, combined with adaptive grouping method, MF-FMA and MLFMA can be used flexibly for different parts of the object simultaneously. MF-FMA is applied for capturing the fine details of the structure accurately, and MLFMA is implemented for the rest of the object. As a result, the memory consumption is greatly reduced compared with MLFMA. Numerical results are performed and compared to verify the AMF-FMA is flexible and efficient.

ACKNOWLEDGMENT

We would like to thank the support of Major State Basic Research Development Program of China (973 Program: 2009CB320201); Natural Science Foundation of 60871013, 60701004, 60928002; Jiangsu Natural Science Foundation of BK2008048.

REFERENCES

[1] S. M. Rao, D. R. Wilton, and A. W. Glisson, "ELectromagnetic scattering by surfaces of arbitrary shape," *IEEE Transactions on Antennas and Propagation.*, vol. 30, no. 3, pp. 409-418, May 1982.

[2] J. M. Jin, *The Finite Element Method in Electromagnetics,* 2nd ed., John Wiley & Sons, Inc., 2002.

[3] W. C. Chew, J. M. Jin, Eric Michielssen, and J. M. Song, *Fast and Efficient Algorithms in Computational*

Electromagnetics, Artech House Publishers, 2001.

[4] L. Greengard, J. F. Huang, V. Rokhlin, and S. Wandzura, "Accelerating fast multipole methods for the Helmholtz equation at low frequencies," *IEEE Comput. Sci. Eng.*, vol. 5, no. 3, pp. 32-38, Jul.-Sep. 1998.

[5] L. J. Jiang and W. C. Chew, "Broad-band fast computational electromagnetics algorithm- MFIPWA," *Proc. 19th Annual Review of Progress in Applied Computational Electromagetics*, pp. 36-41, Mar. 2003.

[6] L. J. Jiang and W. C. Chew, "Low-frequency fast inhomogeneous plane-wave algorithm (LF-FIPWA)," *Microw. Opt. Technol. Lett*., vol. 40, no. 2, pp. 117-122, Jan. 20, 2004.

[7] L. J. Jiang and W. C. Chew, "A Mixed-Form Fast Multipole Algorithm," *IEEE Transactions on Antennas and Propagation,* vol. 53, no. 12, pp. 4145- 4156, Dec.2005.

[8] H. Cheng, L. Greengard, and V. Rokhlin, "A fast Adaptive multipole algorithm in three dimensions," *J. Comput. Phys*., vol. 155, pp. 468-498, 1999.

[9] L. Greengard and V. Rokhlin, "A fast algorithm for particle simulation," *J. Comput. Phys.*, vol. 73, pp. 325-348, 1987.

[10] J. S. Zhao and W. C. Chew, "Three dimensional multilevel fast multipole algorithm from static to electrodynamic," *Micro. Opt. Technol. Lett*., vol. 26, no. 1, pp. 43-48, 2000.

[11] J. S. Zhao and W. C. Chew, "A succinct way to diagonalize the translation matrix in three dimensions," *Micro. Opt. Technol. Lett.*, vol. 15, no. 3, pp. 144-147, 1997.

[12] S. Ayatollahi and M. Safayi Naeini, "Adaptive plane-wave expansion algorithm for efficient computation of electromagnetic fields in low-frequency problems," *Microwaves, Antennas and Propagation, IEE Proceedings*, no. 3, pp.182-190, 2006.

[13] L. J. Jiang, *Studies on low frequency fast multipole algorithms,* Ph.D. Dissertation, University of Illinois, Urbana, 2004.

[14] D. R. Wilton and A. W. Glisson, "On improving the electric field integral equation at low frequencies," *1981 Spring URSI Radio Science Meeting Digest*, pp. 24, June 1981.

[15] J. R. Mautz and R. F. Harrington, "An E-field solution for a conducting surface small or comparable to the wavelength," *IEEE Transactions on Antennas and Propagation.*, vol. 32, no. 4, pp. 330-339, April 1984.

Hua Chen was born in Anhui Province, China. She received the B.S. degree in Electronic Information Engineering from Anhui University, China, in 2005, and is currently working toward the Ph.D. degree at Nanjing University of Science and Technology (NJUST), Nanjing, China. Her current research interests include computational electromagnetics, antennas and electromagnetic scattering and propagation, electromagnetic modeling of microwave integrated circuits.

Zhen-Hong Fan was born in Jiangsu, the People's Republic of China in 1978. He received the M.Sc. and Ph.D. degrees in Electromagnetic Field and Microwave Technique from Nanjing University of Science and Technology (NJUST), Nanjing, China, in 2003 and 2007, respectively. During 2006, he was with the Center of Wireless Communication in the City University of Hong Kong, Kowloon, as a Research Assistant. He is currently an Associated Professor with the Electronic Engineering of NJUST. He is the author or coauthor of over 20 technical papers. His current research interests include computational electromagnetics, electromagnetic scattering, and radiation.

Ru-Shan Chen (M'01) was born in Jiangsu, P. R. China. He received his B.Sc. and M.Sc. degrees from the Dept. of Radio Engineering, Southeast University, in 1987 and in 1990,

respectively, and his Ph.D. from the Dept. of Electronic Engineering, City University of Hong Kong in 2001. He joined the Dept. of Electrical Engineering, Nanjing University of Science & Technology (NJUST), where he became a Teaching Assistant in 1990 and a Lecturer in 1992. Since September 1996, he has been a Visiting Scholar with the Department of Electronic Engineering, City University of Hong Kong, first as Research Associate, then as a Senior Research Associate in July 1997, a Research Fellow in April 1998, and a Senior Research Fellow in 1999. From June to September 1999, he was also a Visiting Scholar at Montreal University, Canada. In September 1999, he was promoted to Full Professor and Associate Director of the Microwave & Communication Research Center in NJUST and in 2007, he was appointed Head of the Dept of Communication Engineering, Nanjing University of Science & Technology. His research interests mainly include microwave/millimeter-wave systems, measurements, antenna, RF-integrated circuits, and computational electromagnetics. He is a Senior Member of the Chinese Institute of Electronics (CIE).

Zhao-Neng Jiang was born in Jiangsu Province, the People's Republic of China in 1985. He received the B.S. degree in Physics from Huaiyin Normal College in 2007, and is currently working toward the Ph.D. degree at Nanjing University of Science and Technology. His research interests focus on fast solution of integral equations, electromagnetic scattering, and propagation.

Meng-Meng Li was born in Jiangsu Province, the People's Republic of China in 1984. He received the B.S. degree in Physics from Huaiyin Normal College in 2007, and is currently working toward the Ph.D. degree at Nanjing University of Science and Technology. His research interests focus on fast solution of integral equations, modeling of microwave integrated circuits, and UWB antennas.